
Beyond Toxic Neurons: A Mechanistic Analysis of DPO for Toxicity Reduction

Yushi Yang*
University of Oxford

Filip Sondej
Jagiellonian University

Harry Mayne
University of Oxford

Adam Mahdi
University of Oxford

Abstract

Safety fine-tuning algorithms are widely used to reduce harmful outputs in language models, but how they achieve this remain unclear. Studying the Direct Preference Optimization (DPO) algorithm for toxicity reduction, current explanations claim that DPO achieves this by dampening the activations of toxic MLP neurons. However, through activation patching, we show that this explanation is incomplete. Projections onto a toxicity probe’s direction show that only 4.9% of toxicity reduction comes from dampened toxic neurons. Instead, DPO reduces toxicity through distributed activation shifts across a majority of neurons, progressively shifting MLP layer outputs away from toxicity. These shifts accumulate across four neuron groups: two reducing toxicity and two promoting anti-toxicity. Activation patching validates the cumulative roles of these groups, where patching all identified groups effectively replicates DPO’s effects. These findings illustrate DPO’s mechanism: it reduces toxicity by accumulating small activation shifts across many neurons throughout the layers. Our findings provide new mechanistic insights into how safety fine-tuning reduces harmful outputs in language models. ²

1 Introduction

The growing capabilities of LLMs also lead to encoding undesirable behaviours, such as producing toxic, biased, or hallucinated outputs. [8, 7, 21]. To address these issues, researchers have developed safety fine-tuning algorithms, such as proximal policy optimization (PPO) [16] and direct preference optimization (DPO) [15], to reduce undesirable outputs.

Recent studies have shown that safety fine-tuning algorithms make minimal parameter changes to pre-trained models, making their underlying capability to generate undesirable outputs retained [12, 10, 11]. However, it remains unclear how such minimal changes lead to a reduction in undesirable outputs. Studying the DPO algorithm for toxicity reduction, the current explanation claims that DPO achieves this by dampening the activations of the most toxic MLP neurons, bypassing the toxic regions they create in the residual stream [12]. However, by tracking the toxic representation identified by a linear probe in MLP neurons, we find this explanation incomplete. Our findings are:

- *Dampened toxic neurons contribute a limited amount to the effect of DPO.* By patching toxic neurons to their post-DPO activations, we observe significantly higher toxicity scores than with DPO, meaning that dampened toxic neurons [12] account for a limited portion of

*Correspondence: Yushi Yang, <yushi.yang@oii.ox.ac.uk>

²The code is available at: <https://github.com/Yushi-Y/dpo-toxic-neurons>.

DPO’s effect. Projections in the direction of the toxicity probe show that they only account for 4.9% of the total toxicity reduction.

- *DPO accumulates small activation shifts across many neurons to reduce toxicity.* DPO induces small activation shifts in most neurons, progressively steering each MLP layer away from toxicity. These shifts come from four neuron groups: two reducing toxicity and two promoting anti-toxicity. Activation patching confirms their cumulative effects, where patching all groups together matches DPO’s toxicity reduction. This illustrates DPO’s mechanism: it induces small activation shifts across many neurons to reduce toxicity writing.

2 Related work

Mechanisms of fine-tuning algorithms Several studies have examined how fine-tuning alters pre-trained model capabilities. Jain et al. [10] found that fine-tuning on synthetic tasks introduces “wrappers” - localised weight adjustments in later layers optimised for specific tasks. Jain et al. [11] showed that safety fine-tuning minimally modifies model weights by projecting unsafe inputs into the null space of the weights. Wei et al. [20] demonstrated the brittleness of safety fine-tuning, where pruning 3% of targeted parameters can unlock the model from aligned behaviours. These findings show that fine-tuning minimally alters model capabilities to produce undesired outputs. However, the exact mechanisms of how these small weight changes lead to behavioural changes remain unclear.

In our reference study, Lee et al. [12] studied how the DPO algorithm reduces toxic outputs. They claimed that DPO reduces toxicity by dampening the activations of toxic MLP neurons, whose value vector (i.e., output weight vectors; see Appendix A) align the most with a toxicity linear probe and project onto toxic tokens. Our study tests this claim and find it limited, as discussed further.

3 Experimental setup

To test Lee et al. [12]’s claim and make fair comparisons, we replicate their experimental setup with the same language model, prompt dataset, probe extraction method, and evaluation metrics.

Model and dataset We use GPT-2 Medium, a 355M-parameter model with 24 layers, a residual stream dimension of 1024, and an MLP hidden layer dimension of 4096 [12]. We use the DPO-tuned version of GPT2-medium [12] fine-tuned on 24,576 pairs of toxicity data generated by PPLM pipeline [3] based on Wikitext-2 prompts. To elicit toxic outputs, we use the “challenge” subset of RealToxicityPrompts [8], which contains 1,199 highly toxic prompts for continued generation.

Toxicity probe We train a linear probe W_{Toxic} at the last layer of GPT2-medium for binary classification of toxic and non-toxic text using the Jigsaw toxic comment classification dataset (561,808 comments) [2]. This probe direction strongly aligns with toxic tokens in the logit lens [14] (see Appendix B) and effectively steers the model in its final layer to reduce toxicity [12]. We interpret this probe as representing the aggregated toxicity information in GPT-2 Medium [12].

Evaluation metrics To evaluate the toxicity and language quality of prompt continuations, we use three metrics: *toxicity scores*, measured by the Perspective API [9] which automatically assigns a toxicity score to each response; *perplexity*, calculated by comparing generated tokens to the Wikitext-2 dataset [13]; and *F1 scores*, calculated by token matches in 2,000 Wikipedia sentences [4].

4 Tracking toxicity reduction across neurons

4.1 Activation patching of toxic neurons

We identify toxic MLP neurons as those whose value vector (Appendix A) have the highest cosine similarity to W_{Toxic} and project onto toxic tokens in the vocabulary space [12]. We narrow this down to $N = 128$ toxic value vectors, as this number forms a stable toxic space identified through singular value decomposition, with additional value vectors failing to expand the toxic basis [12]. Also, for $N > 128$, the value vectors no longer project onto toxic tokens (Appendix B).

Table 1: **Toxicity, Perplexity (PPL) and F1 scores after activation patching.** Patching toxic neurons to post-DPO levels results in limited toxicity reduction compared to DPO. In contrast, patching the neuron groups we identified matches or exceeds DPO in reducing toxicity.

Model	Intervention	Toxicity	PPL	F1
GPT2	None	0.453	21.70	0.193
DPO	None	<u>0.208</u>	23.34	0.195
GPT2	Patch toxic neurons to post-DPO activations	0.404	21.70	0.193
GPT2	Patch positively activated toxic neurons	0.409	21.70	0.193
GPT2	Ablate toxic neurons	0.409	22.13	0.192
GPT2	Ablate positively activated toxic neurons	0.398	21.74	0.193
GPT2	Patch TP₋ group to post-DPO activations	0.335	21.69	0.190
GPT2	Patch TN₊ group to post-DPO activations	0.413	21.71	0.190
GPT2	Patch AN₋ group to post-DPO activations	0.410	21.80	0.193
GPT2	Patch TP₋ and AN₋ to post-DPO activations	0.239	21.78	0.189
GPT2	Patch TP₋ , AN₋ , TN₊ to post-DPO activations	0.193	21.76	0.174
GPT2	Patch all four groups to post-DPO activations	0.114	21.76	0.171

To test the claim by Lee et al. [12], we patch the pre-trained model’s activations for 128 toxic neurons to their post-DPO levels. We also selectively patch 36 of these neurons with positive pre-DPO activations to test the dampening claim, as negative activations cannot be dampened. For a stronger intervention, we ablate the toxic neurons by zeroing out their activations, removing the toxic regions they create in the residual stream. This tests their maximum impact.

Table 1 shows that both patching and ablating toxic neurons yield limited toxicity score reduction compared to DPO. This suggests that dampened toxic neurons account for a small portion of DPO’s impact, and toxicity cannot be solely attributed to a few specific neurons.

4.2 Computing neuron toxicity via projection

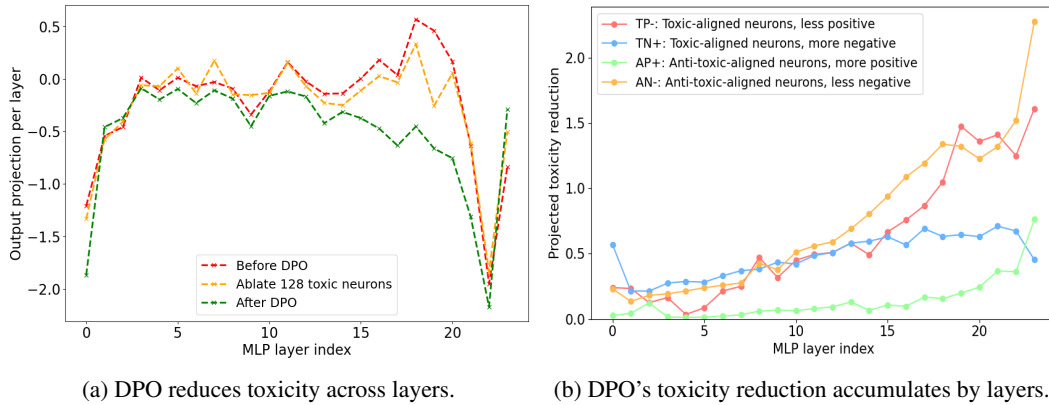


Figure 1: **Toxicity projection across MLP layers.** (a) Toxicity projection consistently drop across layers after DPO, surpassing the reduction by ablating toxic neurons. (b) DPO reduces projected toxicity by combining neuron effects across layers.

To capture neuron-level toxicity change, we first project each MLP block output onto the normalised probe direction W_{Toxic} . These projections are averaged for 1,199 prompts and 20 generated tokens. Figure 1a shows a consistent drop in toxicity projections after DPO, surpassing the drop by ablating toxic neurons across layers.

We then decompose the drop in the MLP output projections (Figure 1a) into per-neuron contributions. Following Equation 3 (in Appendix A), which describes the mechanism of MLP blocks, we attribute

per-layer activation changes to the sum of neuron activation changes within that layer. Specifically, we compute the change in neuron i 's contribution to toxicity after DPO as:

$$\text{toxicity_change}_i = (m_i^{\text{pre}} v_i^{\text{pre}} - m_i^{\text{dpo}} v_i^{\text{dpo}}) \cdot \frac{W_{\text{Toxic}}}{|W_{\text{Toxic}}|}, \quad (1)$$

where m_i^{pre} and m_i^{dpo} are the activation coefficients of neuron i before and after DPO, v_i^{pre} and v_i^{dpo} are corresponding to the value vectors. This equation measures the change in each neuron's toxicity projection following DPO.

Results We find that, while v_i^{pre} and v_i^{dpo} barely change across all neurons during DPO (with an average cosine similarity greater than 0.99 [12]), 58% of all neurons (57,500 neurons) show reduced toxicity projections through subtle activation shifts from m_i^{pre} to m_i^{dpo} . Notably, contributions from toxic neurons with dampened positive activations account for **4.9%** of the total reduction. Additionally, the majority of contributing neurons do not directly project to toxic tokens (Appendix B), indicating that their influence on toxicity arises indirectly through interactions. This suggests that, DPO reduces toxicity by inducing small distributed activation shifts across the majority of neurons.

Figure 1b shows how these activation shifts accumulate across MLP layers (via four neuron groups in Section 4.3) and progressively steer layer outputs away from toxicity. Reduced activations in one layer are passed to the next with adjusted weights, compounding toxicity reduction. This results in the most significant reductions in the later layers, effectively suppressing toxic outputs.

4.3 Neuron groups combine effects to reduce toxicity

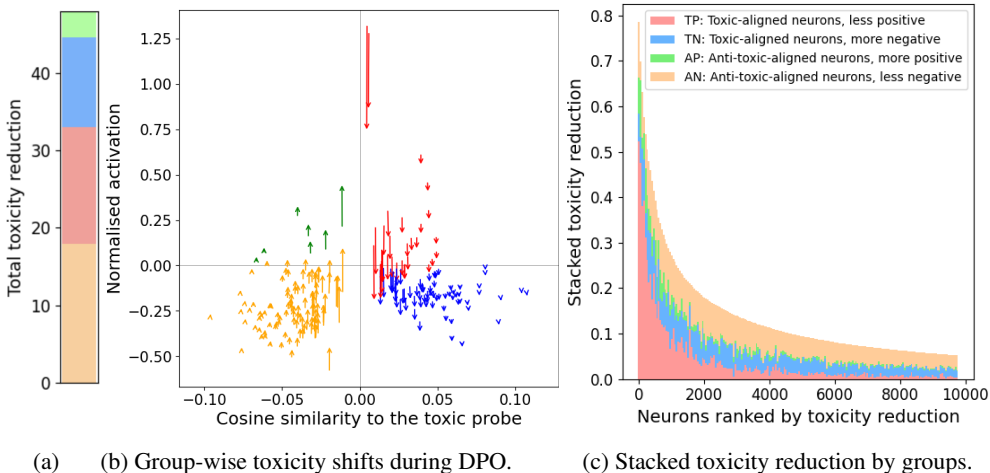


Figure 2: **Four neuron groups combine to reduce toxicity.** (a) Proportions of toxicity reduction by groups; (b) Toxicity shifts for the top 3,000–3,200 contributing neurons, with arrows showing projection changes from pre-DPO to post-DPO; (c) Stacked toxicity reduction of the top 10,000 contributing neurons. **TP₋** initially dominates, **AN₋** gradually catches up as neuron rank progresses.

We analyse how neurons combine effects to reduce toxicity projection, by categorising them into four groups based on two criteria: (1) whether their value vector aligns positively or negatively with the probe direction W_{Toxic} , where we label them as either ‘toxic-aligned’ or ‘anti-toxic-aligned’; (2) whether their activations increase or decrease after DPO.

These criteria produce four groups: (1) Toxic-aligned neurons activated less positively (**TP₋**); (2) Toxic-aligned neurons activated more negatively (**TN₊**); (3) Anti-toxic-aligned neurons activated less negatively (**AN₋**); (4) Anti-toxic-aligned neurons activated more positively (**AP₊**). Note that the dampened toxic neurons [12] belong to the **TP₋** group. Groups **TN₊** and **AN₋** arise due to the small negative activations induced by the GELU activation function (Appendix C).

Figure 2a shows that **TP₋** and **AN₋** are the primary contributing groups, accounting for 69.1% of the total reduction by removing toxicity, while the remaining two groups contribute 30.9% by promoting

anti-toxicity. Figure 2b demonstrates balanced toxicity shifts across groups. Figure 2c highlights how reduction accumulates with neuron ranks: **TP₋** initially dominates, while **AN₋** progressively catches up as later-ranked neurons contribute increasingly to the reduction.

Validate neuron groups We perform activation patching on each group to validate their effects, by adjusting their activations to post-DPO levels and re-measuring toxicity scores using the Perspective API [9]. We apply averaged patching [6], setting each neuron to its mean post-DPO activation value (averaged across all prompts and 20 generated tokens) at the final token position, to guide next-token generation for each prompt.

Table 1 shows that patching each neuron group reduces toxicity. Patching the top two groups (**TP₋** and **AN₋**) achieves a similar level of toxicity reduction as DPO, while patching the top three groups (**TP₋**, **AN₋**, **TN₊**) or all four groups surpasses DPO’s reduction. This validates the cumulative role of neuron groups in reducing toxicity. The superior performance of patching all groups is likely due to the exclusion of neurons that increase toxicity after DPO (Appendix D). Furthermore, our patching technique minimally impact perplexity, showing that the distributed activation shifts induced by DPO preserve general language capabilities.

5 Discussion

How DPO reduces toxicity Based on these findings, we formalise how DPO reduces toxicity. DPO creates minimal weight changes in the pre-trained model [12], which induce distributed activation shifts across neuron groups at each layer, both reducing toxicity and promoting anti-toxicity. The shifted activations in each layer are propagated to the next through adjusted weights, compounding the reduction and resulting in the most significant effects in later layers, effectively suppressing toxic outputs. The minimal weight changes of DPO mean that the underlying model capability to generate toxic outputs remains largely intact [12]. However, these distributed activation shifts induced by DPO effectively limit the activation of these toxic capabilities across layers, thus reducing toxic outputs.

Neuron intervention to replicate DPO Our results show that intervening on a small subset of neurons, such as ablating toxic neurons, is insufficient to replicate the effects of safety fine-tuning. Instead, subtle, distributed interventions across many neurons are more likely to be effective. For example, leveraging insights from DPO, our patching technique on neuron groups successfully reduces toxicity while maintaining low perplexity, effectively replicating DPO’s impact. A similar observation is made by Suau et al. [18].

6 Conclusion

This study decodes how DPO reduces toxic outputs by tracking how writing in a toxic representation is reduced across MLP neurons. We challenge the notion that toxicity reduction is driven by a few toxic neurons [12], which assumes a monosemantic view of neurons—a perspective proven inaccurate [5]. Instead, we find that DPO reduces toxicity through distributed activation shifts across neuron groups, with them cumulative effects to steer each MLP layer away from toxicity. Building on these findings, we propose an activation patching technique on the identified neuron groups to replicate DPO’s toxicity reduction. By examining DPO as a case study, this work provides new mechanistic insights into how safety fine-tuning reduces harmful outputs.

7 Limitations

Our proposed method relies on a single linear probe direction to capture the aggregated toxicity representation, which may miss more nuanced aspects of toxicity. For example, different toxic behaviours, such as gender bias or the use of curse words, may manifest in different directions. Future work could extend our approach by projecting onto a toxic subspace spanned by multiple toxic feature directions, such as those extracted from contrastive pairs [19], to identify more precise neuron groups.

Additionally, we estimate each neuron’s contribution to toxicity using projections, assuming proportional toxicity writing along its activated direction. However, toxic features may be distributed across neurons in a more complex linear composition with varying weights. Alternative approaches,

such as sparse autoencoders (SAEs) [1], could be explored to trace the change of fine-grained toxic features across neurons. Future work could also investigate how interactions between the identified neuron groups influence the model’s toxicity, such as how weight changes drive activation shifts across groups and whether there are any trade-offs involved.

References

- [1] Trenton Bricken, Adly Templeton, Joshua Batson, Brian Chen, Adam Jermyn, Tom Conerly, Nick Turner, Cem Anil, Carson Denison, Amanda Askell, et al. Towards monosemanticity: Decomposing language models with dictionary learning. *Transformer Circuits Thread*, 2, 2023.
- [2] cjadams, Jeffrey Sorensen, Julia Elliott, Lucas Dixon, Mark McDonald, nithum, and Will Cukierski. Toxic comment classification challenge, 2017. URL <https://kaggle.com/competitions/jigsaw-toxic-comment-classification-challenge>. Accessed: 8-Nov-2024.
- [3] Sumanth Dathathri, Andrea Madotto, Janice Lan, Jane Hung, Eric Frank, Piero Molino, Jason Yosinski, and Rosanne Liu. Plug and play language models: A simple approach to controlled text generation, 2020. arXiv: 1912.02164.
- [4] Emily Dinan, Varvara Logacheva, Valentin Malykh, Alexander Miller, Kurt Shuster, Jack Urbanek, Douwe Kiela, Arthur Szlam, Iulian Serban, Ryan Lowe, Shrimai Prabhumoye, Alan W Black, Alexander Rudnicky, Jason Williams, Joelle Pineau, Mikhail Burtsev, and Jason Weston. The second conversational intelligence challenge (convai2), 2019. arXiv: 1902.00098.
- [5] Nelson Elhage, Tristan Hume, Catherine Olsson, Nicholas Schiefer, and Tom Henighan et al. Toy models of superposition, 2022. arXiv:2209.10652.
- [6] Javier Ferrando, Gabriele Sarti, Arianna Bisazza, and Marta R. Costa-jussà. A primer on the inner workings of transformer-based language models, 2024. arXiv: 2405.00208.
- [7] Isabel O. Gallegos, Ryan A. Rossi, Joe Barrow, Md Mehrab Tanjim, Sungchul Kim, Franck Dernoncourt, Tong Yu, Ruiyi Zhang, and Nesreen K. Ahmed. Bias and fairness in large language models: A survey, 2024. arXiv: 2309.00770.
- [8] Samuel Gehman, Suchin Gururangan, Maarten Sap, Yejin Choi, and Noah A. Smith. Re-alextoxicityprompts: Evaluating neural toxic degeneration in language models, 2020. arXiv: 2009.11462.
- [9] Mor Geva, Avi Caciularu, Kevin Ro Wang, and Yoav Goldberg. Transformer feed-forward layers build predictions by promoting concepts in the vocabulary space, 2022. arXiv: 2203.14680.
- [10] Samyak Jain, Robert Kirk, Ekdeep Singh Lubana, Robert P. Dick, Hidenori Tanaka, Edward Grefenstette, Tim Rocktäschel, and David Scott Krueger. Mechanistically analyzing the effects of fine-tuning on procedurally defined tasks, 2023. arXiv: 2311.12786.
- [11] Samyak Jain, Ekdeep Singh Lubana, Kemal Oksuz, Tom Joy, Philip H. S. Torr, Amartya Sanyal, and Puneet K. Dokania. What makes and breaks safety fine-tuning? a mechanistic study, 2024. arXiv: 2407.10264.
- [12] Andrew Lee, Xiaoyan Bai, Itamar Pres, Martin Wattenberg, Jonathan K. Kummerfeld, and Rada Mihalcea. A mechanistic understanding of alignment algorithms: A case study on dpo and toxicity, 2024. arXiv: 2401.01967.
- [13] Stephen Merity, Caiming Xiong, James Bradbury, and Richard Socher. Pointer sentinel mixture models, 2016. arXiv: 1609.07843.
- [14] nostalgebraist. Interpreting GPT: The logit lens. *AI Alignment Forum*, 2020. Accessed: 13-Dec-2024.

- [15] Rafael Rafailov, Archit Sharma, Eric Mitchell, Stefano Ermon, Christopher D. Manning, and Chelsea Finn. Direct preference optimization: Your language model is secretly a reward model, 2024. arXiv: 2305.18290.
- [16] John Schulman, Filip Wolski, Prafulla Dhariwal, Alec Radford, and Oleg Klimov. Proximal policy optimization algorithms, 2017. arXiv: 1707.06347.
- [17] Noam Shazeer. Glu variants improve transformer, 2020. arXiv: 2002.05202.
- [18] Xavier Suau, Pieter Delobelle, Katherine Metcalf, Armand Joulin, and Nicholas Apostoloff et al. Whispering experts: Neural interventions for toxicity mitigation in language models, 2024. arXiv:2407.12824.
- [19] Rheeya Uppaal, Apratim Dey, Yiting He, Yiqiao Zhong, and Junjie Hu. Detox: Toxic subspace projection for model editing, 2024. arXiv: 2405.13967.
- [20] Boyi Wei, Kaixuan Huang, Yangsibo Huang, Tinghao Xie, Xiangyu Qi, Mengzhou Xia, Prateek Mittal, Mengdi Wang, and Peter Henderson. Assessing the brittleness of safety alignment via pruning and low-rank modifications, 2024. arXiv: 2402.05162.
- [21] Yue Zhang, Yafu Li, Leyang Cui, Deng Cai, Lemao Liu, Tingchen Fu, Xinting Huang, Enbo Zhao, Yu Zhang, Yulong Chen, Longyue Wang, Anh Tuan Luu, Wei Bi, Freda Shi, and Shuming Shi. Siren’s song in the ai ocean: A survey on hallucination in large language models, 2023. arXiv: 2309.01219.

A Mechanisms of MLP blocks in Transformers

In this section, we explain mathematically how MLP blocks function in transformer models.

Each MLP block l in a transformer passes the input \mathbf{x}^l through two linear transformations with a point-wise activation function σ in between:

$$\text{MLP}^\ell(\mathbf{x}^\ell) = \sigma(W_K^\ell \mathbf{x}^\ell) W_V^\ell, \quad (2)$$

where $W_K^\ell, W_V^\ell \in \mathbb{R}^{d_{\text{mlp}} \times d}$, d_{mlp} and d are the dimensions of MLP hidden layers and the residual stream, respectively. Expanding the equation gives:

$$\text{MLP}^\ell(\mathbf{x}^\ell) = \sum_{i=1}^{d_{\text{mlp}}} \sigma(\mathbf{x}^\ell \cdot \mathbf{k}_i^\ell) \mathbf{v}_i^\ell = \sum_{i=1}^{d_{\text{mlp}}} m_i^\ell \mathbf{v}_i^\ell. \quad (3)$$

For neuron i , we refer to \mathbf{k}_i^ℓ (the i -th row of W_K^ℓ) as the *key vector*, and \mathbf{v}_i^ℓ (the i -th column of W_V^ℓ) as the *value vector* following [9]. This equation indicates that the MLP layer writes to the residual stream d_{mlp} times, once for each value vector \mathbf{v}_i^ℓ activated by a coefficient m_i^ℓ . According to Geva et al. [9], each sub-update $m_i^\ell \mathbf{v}_i^\ell$ promotes the likelihood of certain tokens being generated in the vocabulary space.

B Projections of value vectors to the vocabulary space

In this section, we show that value vectors cease to project onto tokens in logit lens [14], as their cosine similarity with the toxicity probe W_{toxic} decreases.

Table 2 indicates that value vectors cease projecting onto toxic tokens at approximately $N = 60$.

Table 2: Top tokens that most toxic-aligned value vectors project in the vocabulary space.

WARNING: THESE EXAMPLES ARE HIGHLY OFFENSIVE.

VECTOR	RANK	TOP TOKENS
W_{Toxic}	-	c*nt, f*ck, a**hole, d*ck, wh*re, holes
MLP.v ₁₉ ⁷⁷⁰	1	sh*t, a**, cr*p, f*ck, c*nt, garbage, trash
MLP.v ₁₈ ²⁶⁶⁹	3	degenerate, whining, idiots, stupid, smug
MLP.v ₃ ³⁶⁸⁰	10	se*ist, feminist, Femin, femin, misogyn
MLP.v ₁₃ ²⁵³	18	c*m, d*ck, icles, icle, bo*bs, naughty,
MLP.v ₇ ³³⁵⁸	29	cr*p, whine, sh*t, uphem, shri, bullsh*t
MLP.v ₁₅ ¹⁶⁹⁶	44	death, extermination, Corpse, decap, torture
MLP.v ₆ ³⁹⁷²	50	f*cking, d*mn, sinful, hell, immoral
MLP.v ₁₂ ²⁷⁵⁶	59	burdens, bad, offending, imped, horrible
MLP.v ₁ ²⁰⁵⁷	60	Bench, rodu, Sequ, RIP, Brist, Vers
MLP.v ₂₀ ³¹²³	61	uple, buff, virgin, intangible, nw, illiter
MLP.v ₁₃ ³⁶²⁰	62	Frenchman, youngster, champ, Tex, superstar
MLP.v ₁₇ ³⁰⁶⁴	63	FK, ELS, pes, strings, tor, IDES, ELF, end
MLP.v ₄ ³⁵⁰⁰	75	odan, amaz, aggressive, Beauty, thumbnails
MLP.v ₀ ²⁷²³	90	iless, izens, iban, crawling, aciously, etheless
MLP.v ₁ ⁵⁷²	128	vous, ccoli, weed, ername, Timber, alyses
MLP.v ₈ ³¹⁹²	129	roma, ocker, oley, hiba, osure, urden
MLP.v ₈ ³⁷⁴⁵	130	revolving, Bree, Hoo, dise, Cheong, uay

C Most toxic neurons have negative activations

In this section, we explain why we include a step to ablate only toxic neurons with positive activations in Table 1. Many toxic value vectors have small negative activations, and indiscriminate ablation of all toxic neurons can unintentionally increase toxicity.

Figure 3 displays the average activations of the top 100 toxic neurons (across all prompts and 20 generated tokens) before and after DPO. While the first few neurons show positive activations, most show small negative activations due to the GeLU activation function. Activation functions allowing negative activations are common in modern LLMs for smooth learning, such as SwiGLU [17] in Llama 3 and GEGLU [17] in Gemma.

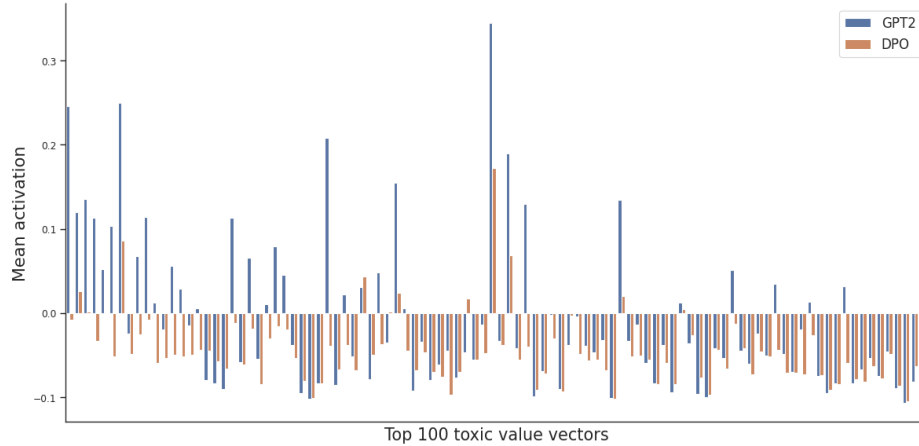


Figure 3: **Activations of the top 100 toxic neurons.** Most neurons have small negative activations before and after DPO due to the GeLU function.

D Many neurons increase toxicity after DPO

In this section, we explore why patching all identified neuron groups achieves a greater toxicity reduction than DPO.

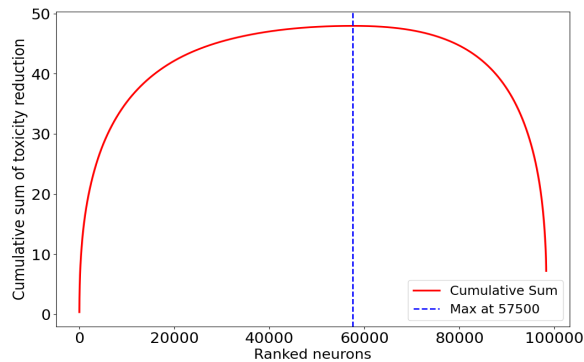


Figure 4: **Cumulative sum of toxicity reduction ranked by neurons.** A significant number of neurons increase toxicity after DPO.

Figure 4 shows that, while DPO adjusts the majority of neurons to reduce toxicity, some neuron activations actually increase toxicity, resulting in a U-shaped curve. This indicates that reducing toxicity in certain neurons comes at the expense of increased toxicity in others, likely due to trade-offs introduced by DPO’s noisy parameter updates. Since we exclude neurons increasing toxicity when patching on all groups, it is likely to outperform DPO in toxicity reduction.

E Toxicity reduction by neuron groups

In this section, we show how neuron groups contribute to toxicity reduction as neuron rank progresses, providing an expanded illustration of Figure 2c.

Figure 5 compares the distribution of top-contributing neurons, focusing on the top 200 neurons versus those ranked between 3000 and 3200. In Figure 5a, **TP₋** dominates among the top 200-contributing neurons. However, as neuron rank progresses, Figure 5b shows increasing contributions from the other three neuron groups, with **AN₋** becoming particularly significant.

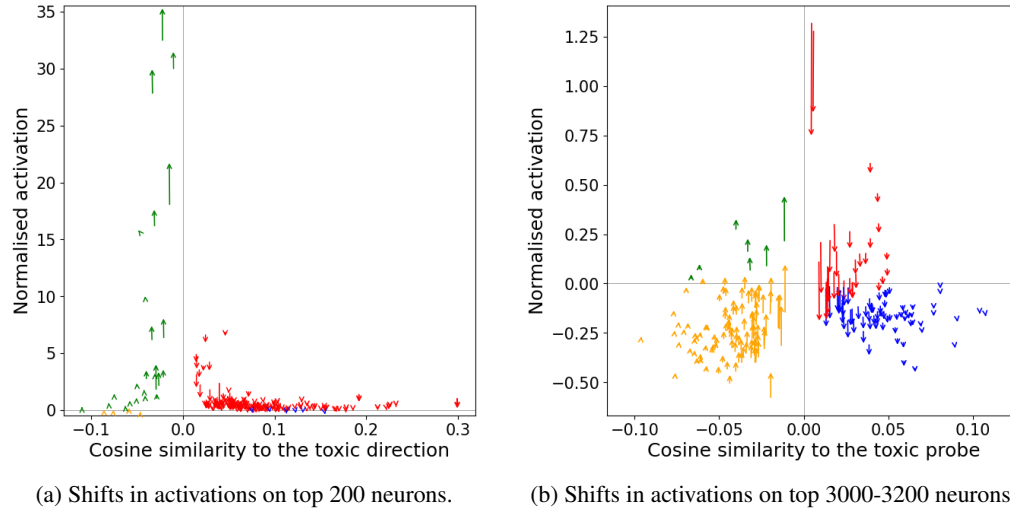


Figure 5: **Shifts in activations of top-contributing neurons.** (a) Among the top 200 neurons, **TP₋** is the primary contributing group. (b) For neurons ranked 3000-3200, contributions are more evenly distributed across all four groups.